Observational signature of continuously operating drivers of decayless kink oscillation

Dong Li[1,2], Zhentong Li[1], Fanpeng Shi[1,3], Yang Su[1], Wei Chen[1], Fu Yu[1,3], Chuan Li[4,5], Ye Qiu[4,5], Yu Huang[1], and Zongjun Ning[1]

[1] Key Laboratory of Dark Matter and Space Astronomy, Purple Mountain Observatory, CAS, Nanjing 210023, China e-mail: `lidong@pmo.ac.cn` & `yang.su@pmo.ac.cn`

[2] State Key Laboratory of Space Weather, Chinese Academy of Sciences, Beijing 100190, PR China

[3] School of Astronomy and Space Science, University of Science and Technology of China, Hefei, 230026, PR China

[4] School of Astronomy and Space Science, Nanjing University, Nanjing 210023, China

[5] Key Laboratory of Modern Astronomy and Astrophysics (Nanjing University), Ministry of Education, Nanjing 210023, China

ABSTRACT

Context. Decayless kink oscillations, which are nearly omnipresent in the solar corona, are believed to be driven by continuously operating energy supply.

Aims. In this letter, we investigate an external continuous excitation of an apparent decayless oscillation during an X1.1 flare on June 20, 2023 (SOL2023-06-20T16:42).

Methods. The decayless kink oscillation was identified in the coronal loop at extreme ultraviolet (EUV) wavelengths and the associated flare quasi-periodic pulsations (QPPs) were simultaneously observed in passbands of hard X-ray (HXR), microwave, and ultraviolet (UV) emissions.

Results. The kink oscillation is detected as a transverse oscillation of the coronal loop, which reveals five apparent cycles with an average period of about 130 ± 10 s. The oscillation amplitude does not show any significantly decay, suggesting a decayless oscillation. At the same time, the solar flare occurs in the vicinity of the oscillating loop and exhibits five main pulses in HXR, microwave, and UV emissions, which could be regarded as flare QPPs. They have similar periods of about 100-130 s, which may indicate successive and repetitive energy releases during the flare impulsive phase. The peak of each loop oscillation cycle appears to follow the pulse of the QPPs, suggesting that the transverse oscillation is closely associated with flare QPPs.

Conclusions. Our observations support the scenario where the repetitive energy released following flare QPPs could be invoked as external, continuously operating drivers of the apparent decayless kink oscillation.

Key words. Sun: flares —Sun: oscillations — Sun: X-rays, gamma rays — Coronal loops — Magnetohydrodynamic (MHD)

1. Introduction

Kink-mode oscillations are usually identified as transverse oscillations of loop-like structures and they are always characterized by non-axisymmetric and weakly compressive in the long-wavelength regime (see Nakariakov et al. 2021, for a recent review). Kink oscillations are well studied magnetohydrodynamic (MHD) waves, since they play a crucial role in diagnosing the solar magnetic field and measuring plasma parameters, namely, "MHD coronal seismology" (e.g., Yuan & Van Doorsselaere 2016; Yang et al. 2020; Chelpanov et al. 2022). They are generally manifested as one of two forms: decaying and decayless oscillations, which are usually dependent on their oscillation amplitudes. The decaying oscillation always reveals a large displacement amplitude, namely, at ≫1 Mm, it decays fast and only persists for several oscillatory cycles. (Nakariakov et al. 1999; Su et al. 2018; Kumar et al. 2022; Li et al. 2023a,b; Zhang et al. 2023). For the large-amplitude oscillation, the decay time is about 1.79 times larger than the oscillation period on average (Nechaeva et al. 2019). Conversely, the decayless oscilla-

tion usually shows small but weakly-decay displacement amplitude, which is less than the minor radius of the oscillating loop (Wang et al. 2012; Anfinogentov et al. 2013; Duckenfield et al. 2018; Mandal et al. 2022). The oscillation periods of standing kink waves are measured from sub-minute to dozens of minutes, and they are linearly increasing with the loop lengths (e.g., Anfinogentov et al. 2015; Nechaeva et al. 2019; Zhang et al. 2022; Petrova et al. 2023; Zhong et al. 2023).

It is well accepted that the kink oscillation should be associated with some external eruptions on the Sun (Nakariakov et al. 2021). The decaying kink oscillation is easily found to be driven by an impulsive driver, for instance, an extreme-ultraviolet (EUV) wave, a solar flare, a flux rope, and a coronal jet (e.g., Zimovets & Nakariakov 2015; Shen et al. 2018, 2019a,b; Reeves et al. 2020). However, the decayless kink oscillation appears to show no apparent association with the solar transient (e.g., Gao et al. 2022; Zhong et al. 2022a; Li & Long 2023). On the other hand, the decayless kink oscillation is nearly omnipresent in the solar atmosphere (Tian et al. 2012; Li et al.

2022a), namely, they are frequently observed in the coronal loop (e.g., Li et al. 2020; Safna Banu et al. 2022), the prominence thread (e.g., Arregui et al. 2018; Li et al. 2018a), the hot flare loop (e.g., Li et al. 2018b; Shi et al. 2023), and the coronal bright point (e.g., Gao et al. 2022). Therefore, they could provide ongoing energy to support the energy loss of the solar corona, which are believed to be crucial for the coronal heating (Van Doorsselaere et al. 2020; Yuan et al. 2023). Obviously, the decayless kink oscillation should also have continuous external drivers to supply that counteracts damping (Zhong et al. 2022a; Nakariakov et al. 2021). In order to answer this issue, several models or mechanisms have been proposed, such as the self-oscillatory model (Nakariakov et al. 2016; Karampelas & Van Doorsselaere 2020), random-motion excitation (Ruderman & Petrukhin 2021), or p-modes exciter (Gao et al. 2023). A series of magnetohydrodynamic (MHD) simulations and theoretical calculations have demonstrated that these models can lead to decayless kink oscillations (Nakariakov et al. 2016; Karampelas & Van Doorsselaere 2020; Ruderman & Petrukhin 2021; Gao et al. 2023). However, capturing observational evidence of continuously operating drivers of decayless kink oscillations is still rare.

Quasi-periodic pulsations (QPPs) are frequently observed in the light curves of solar flares and often associated with MHD waves in solar atmospheres (see Zimovets et al. 2021a, for a recent review). These phenomena could correspond to the quasi-periodic energy release process (e.g., Zimovets et al. 2021b; Li & Chen 2022). A typical QPP is generally characterized by a series of regular and repeated pulses and it could be observed in multiple wavelengths, such as radio, Hα, Lyα, extreme-ultraviolet (EUV), soft and hard X-rays (SXR/HXR), and even γ-rays. The quasi-periods are measured from subseconds to several hundreds seconds (e.g., Nakariakov et al. 2010; Kolotkov et al. 2018; Kashapova et al. 2020; Li et al. 2021; Li 2022; Karlický et al. 2022; Kou et al. 2022; Zhao et al. 2023). The kink oscillation is often observed as the spatial displacement disturbance of loop-like structures, while the QPP refers to the periodic variation of light curves during a solar eruption. Therefore, the kink-mode wave is commonly used to interpret the observed QPP (e.g., Nakariakov et al. 2010; Li et al. 2022b). However, the loop oscillation that is strongly associated with flare QPPs is rarely reported. In this letter, we investigate the decayless kink oscillation of a coronal loop, which could be excited by the repetitive energy releases behind flare QPPs.

2. Observation

We analyzed a coronal loop that was associated with a solar flare occurred on 2023 June 20, which lied in the active region of NOAA 13234 near the solar east limb, namely, S17E73. They were simultaneously measured by the Hard X-ray Imager (HXI; Su et al. 2019; Zhang et al. 2019) on board the Advanced Space-based Solar Observatory[1] (ASO-S; Gan et al. 2023), Konus-Wind (KW; Lysenko et al. 2022), Geostationary Operational Environmental Satellite (GOES), Expanded Owens Valley Solar Array (EOVSA; Gary et al. 2011), STEREO/WAVES (SWAVES), Atmospheric Imaging Assembly (AIA; Lemen et al. 2012) on board the Solar Dynamics Observatory (SDO), and the Chinese Hα Solar Explorer[2] (CHASE; Li et al. 2022; Qiu et al. 2022). Figure 1 shows the light curves in multiple wavelengths during the solar flare. The SXR fluxes at 1-8 Å (red) and 0.5-4 Å

---

[1] http://aso-s.pmo.ac.cn/sodc/dataArchive.jsp
[2] https://ssdc.nju.edu.cn

(blue) are recorded by GOES-18, which has a time cadence of 1 s.

ASO-S/HXI is designed to image solar flares in the HXR energy range of about 15-300 keV. Its time cadence is 4 s in regular observation mode and can be as high as ~0.125 s in burst mode. In this study, we use the full-disk light curve of three total flux monitors (D92, D93, D94) in the range of 20-80 keV interpolated at a time cadence of 1 s from the full cadence light curve, as shown by the magenta line in Figure 1 (b). KW is used for investigating γ-ray bursts and solar flares, which works in two modes: waiting and triggered modes. The count rate light curve has an accumulation time of 2.944 s in the waiting mode, while it has a varying time resolution (e.g., 2-256 ms) in the triggered mode. Therefore, we interpolate the KW flux at 20-80 keV into an uniform cadence of 2.944 s, as indicated by the green line in Figure 1 (b). We also use the radio dynamic spectra measured by EOVSA and SWAVES, as shown by the background images in Figure 1. SWAVES acquires the radio spectrum with a time cadence of 60 s, and it covers a frequency range of roughly 0.05-16.025 MHz. EOVSA is a microwave radioheliograph, which provides the solar spectrum at frequencies of ~1-18 GHz, and the time cadence could be as high as 1 s. We note that some data gaps appear in the EOVSA spectrum.

SDO/AIA takes full-disk solar maps in multiple EUV/UV passbands, and the time cadence of seven EUV passbands is 12 s, while that of two UV passbands is 24 s (Lemen et al. 2012). In this study, we analyze AIA maps in seven passbands of 131 Å (~10 MK), 94 Å (~6.3 MK), 193 Å (~20 MK & ~1.6 MK), 211 Å (~2.0 MK), 171 Å (~0.63 MK), 1600 Å (~0.1 MK), and 1700 Å (~0.005 MK), as shown in Figure 2. All the AIA maps are pre-processed by aia_prep.pro, and have a same spatial resolution of 1.2″. CHASE provides the spectroscopic observation of the full Sun in wavebands of Hα and Fe I (Li et al. 2022). Here, we use the spectral images at channels of Hα 6562.8 Å and Fe I 6569.2 Å, which mainly form in the solar chromosphere and photosphere, respectively. Each spatial pixel corresponds to ~1.04″, and the time cadence is about 71 s.

3. Results

Figure 1 presents the solar flare observed in passbands of SXR, HXR and radio and microwave emissions. Panel (a) shows full-disk light curves at GOES 1-8 Å (red) and 0.5-4.0 Å (blue) from 16:41 UT to 17:30 UT. The GOES flux indicates an X1.1-class flare, which begins at ~16:42 UT, and reach its maximum at ~17:09 UT. The orange line represents the local EUV flux in the wavelength of AIA 131 Å, which is integrated over the flare region. Figure 1 (b) shows HXR and microwave fluxes during 16:56-17:15 UT measured by ASO-S/HXI (magenta), KW (green), and EOVSA (cyan), respectively. Those light curves match well with each other, and they all reveal at least five pulses, which could be regarded as flare QPPs. The background images are radio dynamic spectra observed by SWAVES (a) and EOVSA (b), which show type III radio bursts at the lower and higher frequency ranges, suggesting that nonthermal electrons are accelerated via magnetic reconnections during the flare impulsive phase.

Figure 2 shows the multi-wavelength images with a field of view (FOV) of ~240″×240″. Panels (a)-(c) plot EUV maps in high-temperature wavelengths of AIA 131 Å, 94 Å, and 193 Å, which display some hot flare loops. The gold rectangle outlines the flare region used to integrate the local flux at AIA 131 Å in Figure 1 (a). While panels d-h illustrate the EUV/UV and

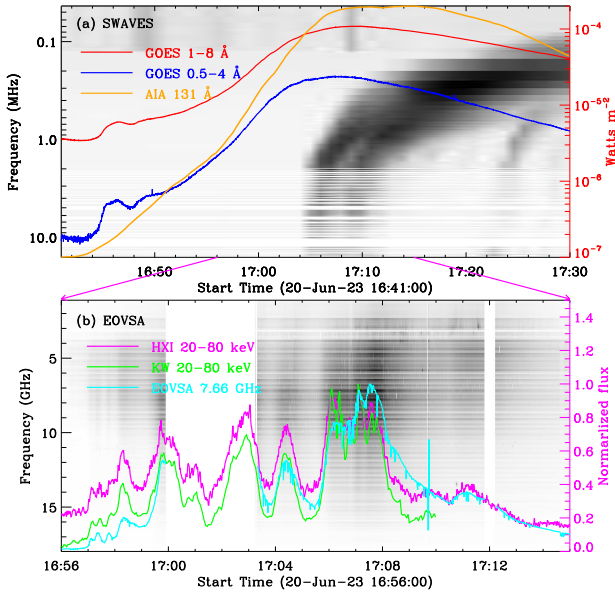**Fig. 1.** Overview of the solar flare on 2023 June 20. a: Full-disk light curves from 16:41 UT to 17:30 UT recorded by GOES at 1-8 Å (red) and 0.5-4 Å (blue), and the local light curve integrated over the flare region measured by SDO/AIA at 131 Å. b: Full-disk light curves between 16:56 UT and 17:15 UT in passbands of HXI 20-80 keV (magenta), KW 20-80 keV (green), and EOVSA 7.66 GHz (cyan). The context images are radio dynamic spectra observed by SWAVES (a) and EOVSA (b), respectively.

Fig. 2. Multi-wavelength snapshots with a FOV of ~240″×240″ measured by SDO/AIA at 131 Å (a), 94 Å (b), 193 Å (c), 171 Å (d), 211 Å (e), 1600 Å (f), and 1700 Å (g), and captured by CHASE in passbands of Hα 6562.8 Å (h) and Fe I 6569.2 Å (i), respectively. The gold box outlines the flare region used to integrate the local flare flux. The cyan arrow indicates the targeted coronal loop, which is used to generate the time-distance map. The magenta contours represents the HXR emission at HXI 30-50 keV, and the contour levels are set 30%, 60%, and 90%. The green contours are derived from the Hα radiation measured by CHASE. An animation that shows the evolution of the solar flare and coronal loop is available online.

Hα maps in passbands of AIA 171 Å, 211 Å, 1600 Å, 1700 Å, and CHASE 6562.8 Å, they all exhibit double flare ribbons and are spatially correlated with two footpoints seen in the HXR emission, as outlined by the green and magenta contours. The HXR map during 17:04:07-17:04:37 UT is reconstructed by the HXI_CLEAN method (pattern-based CLEAN algorithm for HXI), utilizing the detectors from D19 to D91, namely, the sub-collimator group G3 to G10, with a spatial resolution of about 6.5″. We exclude the fine grids of G1 and G2 since they are not calibrated yet and the fine structures are not the focus of this study. It should be pointed out that ASO-S was in calibration mode for other payloads during this flare and was therefore pointing away from the solar disk center. The HXI pointing data was regenerated using a machine-learning method. Panel i presents the CHASE map in the wavelength of Fe I 6569.2 Å, and we can see a sunspot, but no signature of the flare radiation. It is interesting that a bunch of coronal loops can be found in passbands of AIA 171 Å, 211 Å, and 193 Å, as indicated by the cyan arrow.

The online animation (anim.mp4) shows the evolution of the solar flare and the associated coronal loops. It can be seen that the coronal loops appear transverse oscillations follow the flare eruption. In order to capture the appearance of transverse oscillations, one artificial straight slit (S1), which is nearly perpendicular to the loop axis, is selected to generate the time-distance (TD) maps. The cut slit is chosen at the position that is close to the apparent loop apex, where is less overlapping with the neighboring loops, as marked by the cyan arrow in Figure 2. Figure 3 presents the TD maps at slit S1 in passbands of AIA 171 Å, 193 Å, and 211 Å. We can immediately notice that several transverse oscillations appear in these TD maps. Herein, there is only one transverse oscillation that shows five apparent peaks ana-
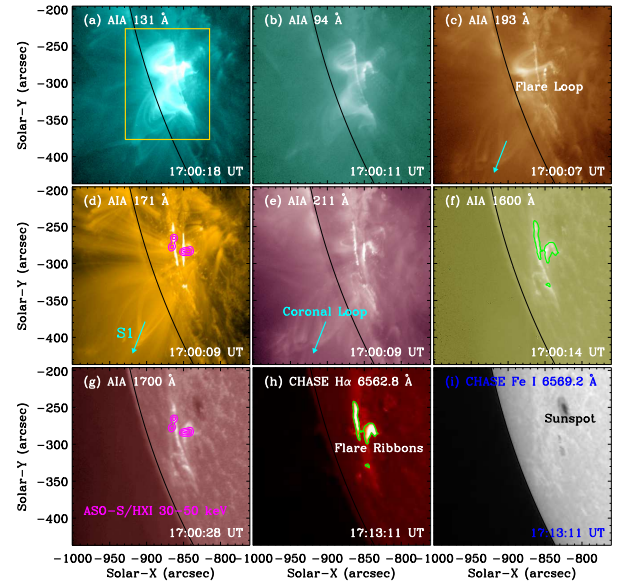
lyzed, since it can be clearly seen in three AIA passbands. Here, the peak of loop oscillation refers to the maximum displacement of transverse oscillations in the TD map. Similarly to previous studies (e.g., Mandal et al. 2021; Zhong et al. 2022b), the oscillation positions are determined from the bright centers of the coronal loop at AIA 171 Å by using the Gaussian fitting method, as marked by the black pluses ('+') in panel (a). The transverse oscillation does not show any apparent decay, but it drifts nonlinearly in the plane-of-sky. Therefore, the combination of a sine function and a nonlinear trend is applied to fit the loop oscillation (e.g., Anfinogentov et al. 2015; Li et al. 2020; Gao et al. 2022; Li & Long 2023), as shown by Equation 1:

$$A(t) = A_m \cdot \sin(\frac{2\pi}{P} t + \psi) + f(t), \qquad (1)$$

Here, A_m represents the displacement amplitude, P is the oscillation period, and ψ refers to the initial phase, while $f(t)$ stands for the second-order polynomial approximation. Next, the velocity amplitude (v_m) is obtained by the derivative of the displacement amplitude (cf. Li et al. 2022a, 2023a; Petrova et al. 2023). The overplotted magenta curve in Figure 3 is the best-fitting result with Equation 1 and it appears to agree with the oscillation positions ('+'). The green line in panel a represents a nonlinear trend of the oscillating loop, which is derived from a second-order polynomial approximation. We want to state that the magenta curve in panels b and c is exactly the same as that in panel a and it seems to be not a good fit in passbands of AIA 193 Å and 211 Å. On the other hand, they appear to match with each other
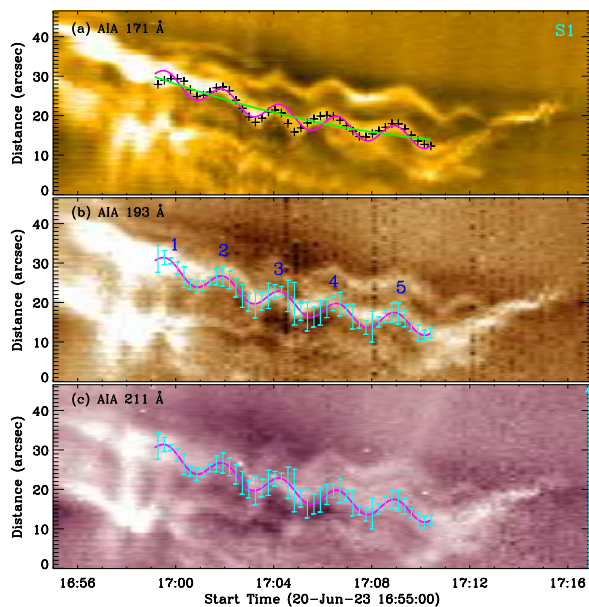
Fig. 3. Time-distance maps show the transverse oscillation of the coronal loop at slit S1 in passbands of AIA 171 Å (a), 193 Å (b), and 211 Å (c). The pluses ('+') outline bright centers of the oscillating loop. The magenta curve and the cyan error bars represent the best-fitting result and their fitting uncertainties, whereas the green line indicates the background trend. The Arabic numerals mark five cycles of the loop oscillation. The cyan arrow indicates the slit direction.

Fig. 4. Oscillating positions ('+') after removing the background trend and its best-fitting result, shown in cyan (a). They are taken from the coronal loop at AIA 171 Å, as shown in Figure 3. The magenta curve shows the HXR flux measured by ASO-S/HXI at 20-80 keV during 16:56-17:15 UT. Local light curve integrated over the flare region (indicated by the gold box in Figure 2) in psaabands of AIA 1700 Å (black), 1600 Å(green), 171 Å (red), and 211 Å (orange), respectively (b). The Arabic and English numbers, as well as the dashed vertical lines outline these oscillating peaks.

when we consider the fitting uncertainty, as shown by the cyan error bars.

Figure 4 (a) presents the oscillating positions ('+') of the coronal loop and the best-fitting result (cyan) after removing the nonlinear trend ($f(t)$), the fitting parameters and their uncertainties such as the oscillation period, displacement and velocity amplitudes are also labeled. The normalized HXR flux at HXI 20-80 keV is also drawn, as shown by the magenta curve. One can immediately notice that both the loop oscillation and the HXR flux reveal at least 5 cycles, as marked by the Arabic and English numbers. The cycle of each HXR pulse appears earlier than that of the loop oscillation, and a time difference of about 110 s was estimated via cross correlation. Those observational facts imply that the transverse oscillation of the coronal loop could be strongly associated with the flare QPP in the HXR channel. We also notice that the HXR flux appears much more small sub-peaks, for instance, the HXR pulse "V" contains three sub-peaks, which might be due to the high time resolution of ASO-S/HXI. We then plot local light curves integrated over the flare region (gold rectangle in Figure 2), as shown in Figure 4 (b). Obviously, the light curves in passbands of AIA 1700 Å (black) and 1600 Å (green) display five apparent peaks, which are almost synchronous with the HXR pulses, as indicated by the dashed vertical lines. On the other hand, the light curves at AIA 171 Å (black) and 211 Å (green) also show five main peaks, while some main peaks also contain sub-peaks, similarly to what has observed in the HXR flux; this suggests the coexistence of multiple periodicities in the flare emission.

In order to identify the quasi-period of flare QPPs, the wavelet transform with the "Morlet" mother function (Torrence & Compo 1998) was applied for the detrended light curves after removing a ~180 s running average (Tian et al. 2012; Li et al. 2018b), since we want to enhance the short-period oscillation and suppress the long-period trend. Figure 5
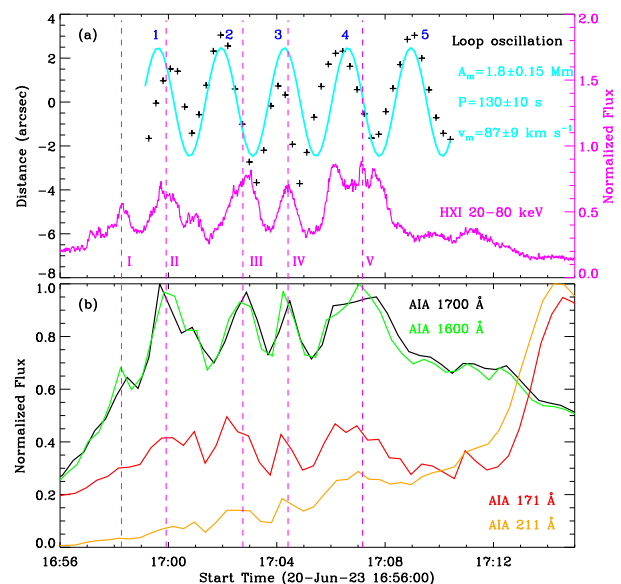
shows the Morlet wavelet power spectra in passbands of HXI 20-80 keV (a), KW 20-80 keV (b), AIA 1700 Å (c), 1600 Å (d), 171 Å (e), and 211 Å (f). They all show an enhanced power over a broad range of quasi-periods, namely, a periodicity range of about 100-130 s. We want to state that the quasi-periods refer to the enhanced power range inside the 99% significance level. The quasi-periods agree with the average period (i.e., ~130±10 s) of the loop oscillation, confirming that the transverse oscillation of the coronal loop could be strongly associated the flare QPPs. We did not perform the wavelet transform for the radio data measured by EOVSA because it has some data gaps, resulting into a discontinuous microwave flux.

4. Discussion

Transverse oscillations are commonly detected in loop-like structures, such as coronal and flare loops, prominence or filament threads, and even umbral fibrils (e.g., Anfinogentov et al. 2015; Nechaeva et al. 2019; Li et al. 2020, 2022a; Zhang et al. 2022; Yuan et al. 2023). In this letter, we study the transverse oscillation of a coronal loop, which is perpendicular to the loop axis at the apparent loop apex. It shows five significant cycles and reveals no apparent decay in the displacement amplitude, which could be regarded as the decayless kink oscillation (Tian et al. 2012; Anfinogentov et al. 2015; Li & Long 2023). The observed kink oscillation shows an average period of ~130±10 s, which is consistent with previous observations that were in the range of tens to hundreds of seconds (Anfinogentov et al. 2015; Li et al. 2020; Mandal et al. 2021; Shi et al. 2022; Zhong et al. 2023). While it has a large displacement amplitude, which is measured to be about 1.8±0.15 Mm. Such a large displacement amplitude is rarely reported in
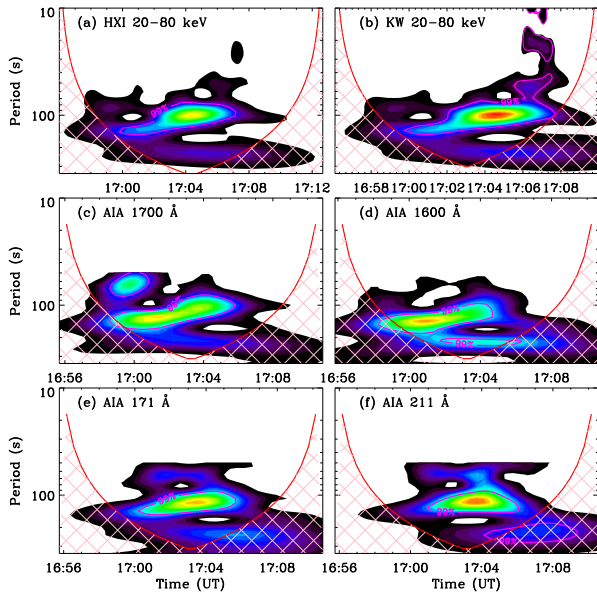
Fig. 5. Morlet wavelet power spectra, as seen in passands of HXI 20-80 keV (a), KW 20-80 keV (b), AIA 1700 Å (c) and 1600 Å (d), 171 Å (e), and 211 Å (f). The magenta contours indicate a significance level of 99%. Anything outside the red curve is dubious.

decayless oscillations. Previous observations found that their displacement amplitude have mostly been less than 0.5 Mm (Anfinogentov et al. 2015; Gao et al. 2022) and the maximal displacement amplitude of 1.16 Mm was detected in decayless kink oscillations induced by a solar flare (cf. Mandal et al. 2021). Li et al. (2020) also reported a decayless kink oscillation with an amplitude of 0.8 Mm. On the other hand, our velocity amplitude is estimated to be 87 km s^{-1} and it is much larger than previous statistical studies for decayless oscillations within longer periods, namely, ~1-8 km s^{-1} (Tian et al. 2012; Gao et al. 2022). Our velocity amplitude is similar to those of decayless oscillations with shorter periods (e.g., Petrova et al. 2023; Li & Long 2023).

A solar flare occurs near the footpoint of the oscillating loop. It shows five repetitive and successive pulses at HXR 20-80 keV measured by ASO-S/HXI and KW, which could be regarded as the signature of flare QPPs. It has a broad range of quasi-periods, such as about 100-130 s. The flare QPPs within similar quasi-periods are also observed in EUV/UV passbands of AIA 1700 Å, 1600 Å, 171 Å, and 211 Å, and these AIA channels show double flare ribbons, which superposed on two HXR footpoints. While those AIA channels at AIA 131 Å, 94 Å and 193 Å do not show the similar QPP feature, since they reveal flare loops. Moreover, some HXR/UV pulses appear to match well with the radio peaks observed by EOVSA, implying the presence of QPP in the microwave emission. Our observations suggest that the flare QPPs are probably caused by repetitive magnetic reconnections (e.g., Kupriyanova et al. 2020; Zimovets et al. 2021a), which could periodically accelerate nonthermal electrons that precipitate into flare footpoints or ribbons. The repeated magnetic reconnections will lead to quasi-periodic energy release processes, namely, five energy releases during the X1.1 flare.

It is interesting that the same periodicity is found between the decayless oscillation and flare QPPs. Moreover, each cycle of the flare QPPs appears earlier than that of the decayless oscillation. Thus, the repetitive energy releases of the X1.1 flare could

be considered as continuously operating drivers of the decayless kink oscillation. The large displacement amplitude could be attributed to the X1.1 flare, which could release a large amount of energies. This is different from previous observations of large-amplitude decayless oscillations that were triggered by small flares (Mandal et al. 2021) or small reconnection events (Li et al. 2020). Mandal et al. (2021) found that the solar flare could only increase oscillation amplitudes but did not change the oscillation nature (see also Shi et al. 2022). However, these studies did not show a distinct one-to-one correspondence over time. In our case, the energy flow appears as "an external driver" induced by a single flare energy release, leading to a large-amplitude kink oscillation of the coronal loop, followed by plasma heating caused by rapid damping (i.e., one oscillation cycle). This process is repeated five times, since the solar flare shows five energy releases via repetitive magnetic reconnections. This model could also explain the small-amplitude decayless oscillation, supposing that the external drivers are continuously existing. However, those external drivers are difficult to observe, mainly because of their fine scales.

Here, we assume the similar damping mechanism in decayless oscillations with the decaying oscillations and it is compensated with continuous energy supply from the ongoing flare energy releases. Then, we can construct an equation like:

$$E(t) = \frac{1}{2}(\rho_i\, v_m^2 + \frac{b^2}{\mu_0}) \cdot e^{-t/\tau}, \qquad (2)$$

where $E(t)$ represents the energy (kinetic + magnetic) density averaged over the oscillation cycle, τ, is the decaying time measured for the displacement amplitude, while v_m, ρ_i, and b are the velocity amplitude, plasma density and magnetic field perturbation, respectively. Then, its derivative $\frac{dE(t)}{dt}$ at t=0 will give us an estimation for the oscillation energy losses (ε):

$$\varepsilon = \frac{dE(t)}{dt} = \frac{1}{2\tau}(\rho_i\, v_m^2 + \frac{b^2}{\mu_0}), \qquad (3)$$

In this study, we know that the decayless oscillation has five oscillation cycles, which correspond to five-cycle energy releases from the flare. If the oscillating loop is affected by a periodic force with the oscillation period, the effect of the resonance must take place and the oscillation amplitude would grow over time (Nakariakov et al. 2009). However, the observed amplitude remains constant, suggesting that the wave energy of each oscillation cycle could completely dissipate at a time scale shorter than or approximately equal to one oscillation period, namely, $\tau \leq P$. According to the resonant absorption theory (Goossens et al. 2002), such a short decay time indicates an abnormal ratio of the loop radius and thickness of the transition layer or an abnormal density ratio inside and outside the loop, either too dense or too rarified. Possible supporting observational evidence to this interpretation is the half-cycle transverse perturbation of the outer loop in Ning et al. (2022). In this work, measuring the loop density may answer this concern but out of the scope of this work. Nevertheless, additional observations and numerical simulations in this direction are necessary for further investigation in the future.

5. Summary

Using the observations from SDO/AIA, ASO-S/HXI, KW, CHASE, EOVSA, SWAVES, and GOES, we investigated an apparent decayless kink oscillation and the associated flare QPPs. Our main conclusions are summarized as follows:

(1) The apparent decayless kink oscillation can be simultaneously seen in passbands of AIA 171 Å, 193 Å, and 211 Å, indicating that the oscillating loop is multi-thermal in nature. The oscillation period is measured to be about 130±10 s and the displacement amplitude is as large as ∼1.8±0.15 Mm.

(2) The flare QPPs are simultaneously detected in passbands of HXI 20-80 keV, KW 20-80 keV, AIA 1700 Å, 1600 Å, 171 Å, and 211 Å during the flare impulsive phase, which might be caused by repetitive magnetic reconnections. The quasi-period is estimated to be ∼100-130 s. The large period range implies the co-existence of multiple periodicities.

(3) The apparent decayless kink oscillation and flare QPPs share the same quasi-period and a significant time difference of about 110 s can be seen between them. Those observational facts provide sufficient evidences that the decayless kink oscillation could be driven by continuously operating energies released from the X1.1 flare.

(4) We propose that the repetitive energy releases behind the flare QPPs could trigger the kink oscillation intermittently for five times, making it apparent decayless. In this interpretation, each cycle of the kink oscillation is assumed to decay rapidly in less than one oscillation period.

References

Anfinogentov, S., Nisticò, G., & Nakariakov, V. M. 2013, A&A, 560, A107. doi:10.1051/0004-6361/201322094

Anfinogentov, S. A., Nakariakov, V. M., & Nisticò, G. 2015, A&A, 583, A136. doi:10.1051/0004-6361/201526195

Arregui, I., Oliver, R., & Ballester, J. L. 2018, Living Reviews in Solar Physics, 15, 3. doi:10.1007/s41116-018-0012-6

Chelpanov, M., Anfinogentov, S., Kostarev, D., et al. 2022, Solar-Terrestrial Physics, 8, 3. doi:10.12737/stp-84202201

Duckenfield, T., Anfinogentov, S. A., Pascoe, D. J., et al. 2018, ApJ, 854, L5. doi:10.3847/2041-8213/aaaaeb

Gan, W., Zhu, C., Deng, Y., et al. 2023, Sol. Phys., 298, 68. doi:10.1007/s11207-023-02166-x

Gao, Y., Tian, H., Van Doorsselaere, T., et al. 2022, ApJ, 930, 55. doi:10.3847/1538-4357/ac62cf

Gao, Y., Guo, M., Van Doorsselaere, T., et al. 2023, arXiv:2308.13813. doi:10.48550/arXiv.2308.13813

Goossens, M., Andries, J., & Aschwanden, M. J. 2002, A&A, 394, L39. doi:10.1051/0004-6361:20021378

Gary, D. E., Hurford, G. J., Nita, G. M., et al. 2011, AAS/Solar Physics Division Abstracts 42

Karampelas, K. & Van Doorsselaere, T. 2020, ApJ, 897, L35. doi:10.3847/2041-8213/ab9f38

Kashapova, L. K., Kupriyanova, E. G., Xu, Z., et al. 2020, A&A, 642, A195. doi:10.1051/0004-6361/201833947

Karlický, M., Rybák, J., Benáček, J., et al. 2022, Sol. Phys., 297, 54. doi:10.1007/s11207-022-01989-4

Kolotkov, D. Y., Pugh, C. E., Broomhall, A.-M., et al. 2018, ApJ, 858, L3. doi:10.3847/2041-8213/aabde9

Kou, Y., Cheng, X., Wang, Y., et al. 2022, Nature Communications, 13, 7680. doi:10.1038/s41467-022-35377-0

Kumar, P., Nakariakov, V. M., Karpen, J. T., et al. 2022, ApJ, 932, L9. doi:10.3847/2041-8213/ac6e3e

Kupriyanova, E., Kolotkov, D., Nakariakov, V., et al. 2020, Solar-Terrestrial Physics, 6, 3. doi:10.12737/stp-61202001

Lemen, J. R., Title, A. M., Akin, D. J., et al. 2012, Sol. Phys., 275, 17. doi:10.1007/s11207-011-9776-8

Li, C., Fang, C., Li, Z., et al. 2022, Science China Physics, Mechanics, and Astronomy, 65, 289602. doi:10.1007/s11433-022-1893-3

Li, D., Shen, Y., Ning, Z., et al. 2018a, ApJ, 863, 192. doi:10.3847/1538-4357/aad33f

Li, D., Yuan, D., Su, Y. N., et al. 2018b, A&A, 617, A86. doi:10.1051/0004-6361/201832991

Li, D., Li, Y., Lu, L., et al. 2020, ApJ, 893, L17. doi:10.3847/2041-8213/ab830c

Li, D., Ge, M., Dominique, M., et al. 2021, ApJ, 921, 179. doi:10.3847/1538-4357/ac1c05

Li, D., Xue, J., Yuan, D., et al. 2022a, Science China Physics, Mechanics, and Astronomy, 65, 239611. doi:10.1007/s11433-021-1836-y

Li, D., Shi, F., Zhao, H., et al. 2022b, Frontiers in Astronomy and Space Sciences, 9, 1032099. doi:10.3389/fspas.2022.1032099

Li, D. 2022, Science in China E: Technological Sciences, 65, 139. doi:10.1007/s11431-020-1771-7

Li, D. & Chen, W. 2022, ApJ, 931, L28. doi:10.3847/2041-8213/ac6fd2

Li, D. & Long, D. M. 2023, ApJ, 944, 8. doi:10.3847/1538-4357/acacf4

Li, D., Bai, X., Tian, H., et al. 2023a, A&A, 675, A169. doi:10.1051/0004-6361/202245812

Li, D., Hou, Z., Bai, X., et al. 2023, arXiv:2311.08767. doi:10.48550/arXiv.2311.08767

Lysenko, A. L., Ulanov, M. V., Kuznetsov, A. A., et al. 2022, ApJS, 262, 32. doi:10.3847/1538-4365/ac8b87

Mandal, S., Tian, H., & Peter, H. 2021, A&A, 652, L3. doi:10.1051/0004-6361/20214154

Mandal, S., Chitta, L. P., Antolin, P., et al. 2022, A&A, 666, L2. doi:10.1051/0004-6361/202244403

Nakariakov, V. M., Ofman, L., Deluca, E. E., et al. 1999, Science, 285, 862. doi:10.1126/science.285.5429.862

Nakariakov, V. M., Aschwanden, M. J., & van Doorsselaere, T. 2009, A&A, 502, 661. doi:10.1051/0004-6361/200810847

Nakariakov, V. M., Foullon, C., Myagkova, I. N., et al. 2010, ApJ, 708, L47. doi:10.1088/2041-8205/708/1/L47

Nakariakov, V. M., Anfinogentov, S. A., Nisticò, G., et al. 2016, A&A, 591, L5. doi:10.1051/0004-6361/201628850

Nakariakov, V. M., Anfinogentov, S. A., Antolin, P., et al. 2021, Space Sci. Rev., 217, 73. doi:10.1007/s11214-021-00847-2

Nechaeva, A., Zimovets, I. V., Nakariakov, V. M., et al. 2019, ApJS, 241, 31. doi:10.3847/1538-4365/ab0e86

Ning, Z., Wang, Y., Hong, Z., et al. 2022, Sol. Phys., 297, 2. doi:10.1007/s11207-021-01935-w

Petrova, E., Magyar, N., Van Doorsselaere, T., et al. 2023, ApJ, 946, 36. doi:10.3847/1538-4357/acb26a

Qiu, Y., Rao, S., Li, C., et al. 2022, Science China Physics, Mechanics, and Astronomy, 65, 289603. doi:10.1007/s11433-022-1900-5

Ruderman, M. S. & Petrukhin, N. S. 2021, MNRAS, 501, 3017. doi:10.1093/mnras/staa3816

Reeves, K. K., Polito, V., Chen, B., et al. 2020, ApJ, 905, 165. doi:10.3847/1538-4357/abc4e0

Safna Banu, K., Maurya, R. A., & Jain Jacob, P. T. 2022, Sol. Phys., 297, 134. doi:10.1007/s11207-022-02065-7

Shen, Y., Tang, Z., Li, H., et al. 2018, MNRAS, 480, L63. doi:10.1093/mnrasl/sly127

Shen, Y., Qu, Z., Yuan, D., et al. 2019a, ApJ, 883, 104. doi:10.3847/1538-4357/ab3a4d

Shen, Y., Qu, Z., Zhou, C., et al. 2019b, ApJ, 885, L11. doi:10.3847/2041-8213/ab4cf3

Shi, F., Ning, Z., & Li, D. 2022, Research in Astronomy and Astrophysics, 22, 105017. doi:10.1088/1674-4527/ac8f8a

Shi, M., Li, B., Chen, S.-X., et al. 2023, ApJ, 943, L19. doi:10.3847/2041-8213/acb3c6

Su, W., Guo, Y., Erdélyi, R., et al. 2018, Scientific Reports, 8, 4471. doi:10.1038/s41598-018-22796-7

Su, Y., Liu, W., Li, Y.-P., et al. 2019, Research in Astronomy and Astrophysics, 19, 163. doi:10.1088/1674-4527/19/11/163

Tian, H., McIntosh, S. W., Wang, T., et al. 2012, ApJ, 759, 144. doi:10.1088/0004-637X/759/2/144

Torrence, C. & Compo, G. P. 1998, Bulletin of the American Meteorological Society, 79, 61. doi:10.1175/1520-0477(1998)079<0061:APGTWA>2.0.CO;2

Van Doorsselaere, T., Srivastava, A. K., Antolin, P., et al. 2020, Space Sci. Rev., 216, 140. doi:10.1007/s11214-020-00770-y

Wang, T., Ofman, L., Davila, J. M., et al. 2012, ApJ, 751, L27. doi:10.1088/2041-8205/751/2/L27

Yang, Z., Tian, H., Tomczyk, S., et al. 2020, Science in China E: Technological Sciences, 63, 2357. doi:10.1007/s11431-020-1706-9

Yuan, D. & Van Doorsselaere, T. 2016, ApJS, 223, 23. doi:10.3847/0067-0049/223/2/23

Yuan, D., Fu, L., Cao, W., et al. 2023, Nature Astronomy. doi:10.1038/s41550-023-01973-3

Zhang, Q., Li, C., Li, D., et al. 2022, ApJ, 937, L21. doi:10.3847/2041-8213/ac8e01

Zhang, Q., Zhou, Y., Li, C., et al. 2023, ApJ, 951, 126. doi:10.3847/1538-4357/acd5cf

Zhang, Z., Chen, D.-Y., Wu, J., et al. 2019, Research in Astronomy and Astrophysics, 19, 160. doi:10.1088/1674-4527/19/11/160

Zhao, H.-S., Li, D., Xiong, S.-L., et al. 2023, Science China Physics, Mechanics, and Astronomy, 66, 259611. doi:10.1007/s11433-022-2064-6

Zhong, S., Nakariakov, V. M., Kolotkov, D. Y., et al. 2022a, MNRAS, 513, 1834. doi:10.1093/mnras/stac1014

Zhong, S., Nakariakov, V. M., Kolotkov, D. Y., et al. 2022b, MNRAS, 516, 5989. doi:10.1093/mnras/stac2545

Zhong, S., Nakariakov, V. M., Miao, Y., et al. 2023, Scientific Reports, 13, 12963. doi:10.1038/s41598-023-40063-2

Zimovets, I. V. & Nakariakov, V. M. 2015, A&A, 577, A4. doi:10.1051/0004-6361/201424960

Zimovets, I. V., McLaughlin, J. A., Srivastava, A. K., et al. 2021a, Space Sci. Rev., 217, 66. doi:10.1007/s11214-021-00840-9

Zimovets, I., Sharykin, I., & Myshyakov, I. 2021b, Sol. Phys., 296, 188. doi:10.1007/s11207-021-01936-9